Cell Reports
Article

Structures of the Sgt2/SGTA Dimerization Domain with the Get5/UBL4A UBL Domain Reveal an Interaction that Forms a Conserved Dynamic Interface

Justin W. Chartron,[1] David G. VanderVelde,[1] and William M. Clemons, Jr.[1,*]
[1]Division of Chemistry and Chemical Engineering, California Institute of Technology, Pasadena, CA 91125, USA
*Correspondence: clemons@caltech.edu
http://dx.doi.org/10.1016/j.celrep.2012.10.010

SUMMARY

In the cytoplasm, the correct delivery of membrane proteins is an essential and highly regulated process. The posttranslational targeting of the important tail-anchor membrane (TA) proteins has recently been under intense investigation. A specialized pathway, called the guided entry of TA proteins (GET) pathway in yeast and the transmembrane domain recognition complex (TRC) pathway in vertebrates, recognizes endoplasmic-reticulum-targeted TA proteins and delivers them through a complex series of handoffs. An early step is the formation of a complex between Sgt2/SGTA, a cochaperone with a presumed ubiquitin-like-binding domain (UBD), and Get5/UBL4A, a ubiquitin-like domain (UBL)-containing protein. We structurally characterize this UBD/UBL interaction for both yeast and human proteins. This characterization is supported by biophysical studies that demonstrate that complex formation is mediated by electrostatics, generating an interface that has high-affinity with rapid kinetics. In total, this work provides a refined model of the interplay of Sgt2 homologs in TA targeting.

INTRODUCTION

Two homologous pathways have been elucidated for the targeting of tail-anchor membrane (TA) proteins to the endoplasmic reticulum (ER) (recently reviewed in Chartron et al., 2012a; Denic, 2012; Hegde and Keenan, 2011). The best characterized is the fungal guided entry of TA proteins (GET) pathway. In its simplest form, a TA sorting complex comprising Sgt2, Get4, and Get5 (alternatively named Mdy2) facilitates the loading of a TA substrate onto the Get3 ATPase. The Get3/TA complex is targeted to the ER, where the TA is released for insertion by the membrane proteins Get1 and Get2. Vertebrates have a related system, referred to as the transmembrane domain recognition complex (TRC) pathway. In this case, the sorting complex similarly contains the proteins TRC35 and UBL4A (alternatively named GDX), homologs of Get4 and Get5, respectively; however, they form a three-component complex with the protein BAG6 (alternatively named BAT3 or Scythe) that is referred to as the BAG6 complex. From here, the TA is handed to a Get3 homolog, TRC40, that delivers the protein to WRB, a homolog of Get1.

Sgt2, a heat-shock protein (HSP) cochaperone, facilitates the first committed step in TA protein targeting. It has been linked genetically and physically to the GET pathway in multiple studies (Battle et al., 2010, Costanzo et al., 2010; Liou et al., 2007; Wang et al., 2010). It recruits a variety of HSP families via an internal tetratricopeptide repeat (TPR) domain (Chartron et al., 2011; Wang et al., 2010). The Sgt2 C-terminal domain can bind to sequences of six or more hydrophobic residues (Liou and Wang, 2005). This includes the transmembrane domain of ER-destined TA proteins that are subsequently transferred to Get3, a process that requires the Get4/Get5 complex (Wang et al., 2010). Mitochondrial TA proteins, which can also copurify with the Sgt2/Get4/Get5 complex, are associated with bound HSPs and are not transferred to Get3 (Wang et al., 2010). The role of Sgt2 in sorting between target organelles is supported by the mislocalization of ER resident TA proteins to the mitochondria in *Δsgt2* cells (Costanzo et al., 2010). The C-terminal domain, which is rich in asparagine, glutamine, and methionine, contains only a short conserved sequence and is weakly predicted as helical. A small N-terminal homodimerization domain (Sgt2-N) mediates the association with a single copy of Get5, providing the link to the rest of the GET pathway (Kohl et al., 2011; Chang et al., 2010; Chartron et al., 2011; Liou et al., 2007). By immunoprecipitation from yeast lysate, the majority of Get5 is associated with Sgt2 (Wang et al., 2010).

Get4 and Get5 form the adaptor that is required for the transfer of TA proteins from Sgt2 to Get3 (Wang et al., 2010). Get4 forms a complex with the N-terminal domain of Get5 and sequesters a nucleotide-bound Get3 (Bozkurt et al., 2010; Chang et al., 2010; Chartron et al., 2010). Get5 has a central ubiquitin-like domain (Get5-UBL) that binds Sgt2-N, and a C-terminal homodimerization domain, resulting in an extended Get4/Get5 heterotetrameric complex (Chartron et al., 2010, 2012b). The complex between Get5 and Sgt2 can be disrupted in vitro by a pair of mutations to the UBL domain that also lead to incomplete rescue of *Δget5* growth defects under stress conditions (Chartron et al., 2010). Moreover, the TA protein transfer reaction is competed by excess Get5, which cannot alone form a productive complex with Get3 (Wang et al., 2010). These results underscore the importance of the physical interaction between Sgt2 and the Get4/Get5 complex. The details of the transfer of TA proteins, including energetic requirements and the in vivo stoichiometry

of Sgt2, Get4/Get5, and Get3 over the course of the handoff, remain to be established.

SGTA, the human homolog of Sgt2, associates with the BAG6 complex through its N terminus (Winnefeld et al., 2006), and UBL4A is postulated to bridge this interaction (Chartron et al., 2012a; Hegde and Keenan, 2011). The BAG6 complex is required for loading TA proteins onto TRC40 (Leznicki et al., 2010; Mariappan et al., 2010), and is also involved in the degradation of membrane proteins in the cytoplasm (Hessa et al., 2011; Minami et al., 2010; Wang et al., 2011).

In this report, we use a combination of structural biology and biochemistry to define the interaction between Sgt2 and Get5, which is conserved from yeast to humans. We now present structures of the N-terminal homodimerization domains from two homologs, yeast Sgt2 and human SGTA, and characterize their fold as a new class of UBD. Further, we solve the structure of the central domain of Get5, demonstrating it as a novel UBL. Finally, we determined the structure of the complex between an Sgt2-N homodimer and the Get5-UBL, revealing an interaction strongly influenced by electrostatics. We used a variety of methods to demonstrate that this interaction has high affinity with rapid binding kinetics. This work provides a critical context for understanding the Sgt2/Get4/Get5 complex, and in addition describes a mechanism for membrane protein entry in the seemingly more complicated mammalian system.

RESULTS

Structures of the Sgt2 and SGTA Dimerization Domains

The Sgt2-N domain is both a homodimerization domain and a binding platform for the Get5-UBL domain. This provides the physical link between the Sgt2 chaperone complex and the GET pathway. Sgt2-N does not have sequence homology to any known structures or other characterized UBDs. To understand how these dual functions are accomplished, we first determined the structure of the *Saccharomyces cerevisiae* Sgt2-N homodimer using solution nuclear magnetic resonance (NMR). The statistics for the NMR structure calculations are provided in Table S1. A monomer of Sgt2-N consists of three helices (Figures 1A–1C). The first two helices are of similar length and mediate homodimerization, forming a four-helix bundle with 2-fold symmetry, consistent with the postulated coiled-coil (Tobaben et al., 2003). A third, shorter helix packs against either side of the bundle away from the dimer interface. The residues C-terminal to this helix, which form the linker to the TPR domain, give weaker signals than the helical region in all NMR experiments, and therefore only partial chemical shift assignments were possible. This is due to different rates of motion relative to the rest of the protein, rather than to proteolysis, as signals for the terminal residues are observed. The few nuclear Overhauser effect (NOE)-derived contacts observed in this sequence restrain it in partially folded conformations (Figure 1C).

The symmetry axis places the equivalent helices from each subunit head to tail, resulting in two unique surfaces. We designate the surface composed of the α2 helices as the "Get5 binding surface," and the opposite surface, composed of the α1 helices, as the "α1 surface" (Figures 1B, 1C, S1A, and S1B). The dimer contacts between α2 helices are made by conserved small residues (Ser32, Ala36, Cys39, and Ala43), resulting in close packing between the main chains of the two subunits (Figure 1B). Cys39 and Val35 make a small hydrophobic patch at the center of the Get5-binding surface (Figures 1A and 1D). The partially exposed Cys39 is strictly conserved across eukaryotes, and Val35 is fully solvent exposed, conserved as either valine or isoleucine (Figure 1G). Despite the close proximity of the Cys39 sulfhydryl groups (5.3 $\pm$ 0.4 Å sulfur-sulfur distance), the C_β shifts of 27.819 ppm argue against disulfide bond formation, even after incubation for several months (Sharma and Rajarathnam, 2000). The conserved acidic residues Asp28 and Glu31 and the conserved positioning of Glu42, Glu47, and Glu49 result in a negatively charged ring surrounding the hydrophobic patch (Figures 1A and 1E).

The dimer contacts between α1 helices are held farther apart than the α2 helices by the interlocking of large hydrophobic side chains (Figures 1B and S1A). This results in an exposed hydrophobic face at the α1 surface that is protected from solvent, to some extent, by the partially folded carboxyl terminal linker (Figures 1C and S1B). When an Sgt2-N variant with this linker deleted is purified, it forms a higher order oligomer, likely due to aggregation at this face (data not shown).

We also investigated the N-terminal domain of human SGTA (SGTA-N). The domain was coexpressed and purified with an affinity-tagged UBL domain of UBL4A (UBL4A-UBL), demonstrating a complex that could be separated from excess UBL4A (Figure S1C). We attempted to crystallize this complex; however, in the three resulting distinct crystal structures, only density for SGTA-N was observed. We determined the structures by molecular replacement using Sgt2-N at 1.35–1.45 Å resolutions. The structures differ predominantly by a postpurification oxidation of the conserved cysteine with buffer components (Figures S1E and S1F). Crystallographic data collection and refinement statistics are provided in Table S2. SGTA-N shares the four-helix bundle topology with Sgt2-N (Figure 1F). As expected from the Sgt2-N solution data, the cysteine sulfhydryl groups do not form a disulfide bond between subunits.

As was the case for structures of the Sgt2/SGTA-TPR domains (Chartron et al., 2011; Dutta and Tan, 2008), Sgt2-N and SGTA-N have very similar architecture with an rmsd of 1.24 $\pm$ 0.07 Å over equivalent C_α atoms (Figure 1F). The sequences have high homology (Figure 1G) and all of the general features are conserved, including the hydrophobic patch surrounded by charge at the binding face (Figures 1F and S1D). One difference is that SGTA-N does not have a third α-helix. The residues that would correspond to α3 are disordered or involved in nonphysiological crystallographic contacts.

Structure of the Get5-UBL Domain

The solution NMR structure of the UBL4A-UBL domain showed that it has the expected ubiquitin fold (Figure 2A; PDB ID: 2DZI; RIKEN Structural Genomics Initiative). Get5-UBL has several small sequence insertions, suggesting some structural differences (Figure 2F); therefore, to fully characterize the yeast system, we determined the structure of the Get5-UBL domain. Initially, we solved a structure by solution NMR (Figure S2A). Simultaneously, we obtained crystals of Get5-UBL that diffracted to 2.4 Å resolution. We were able to obtain phases by

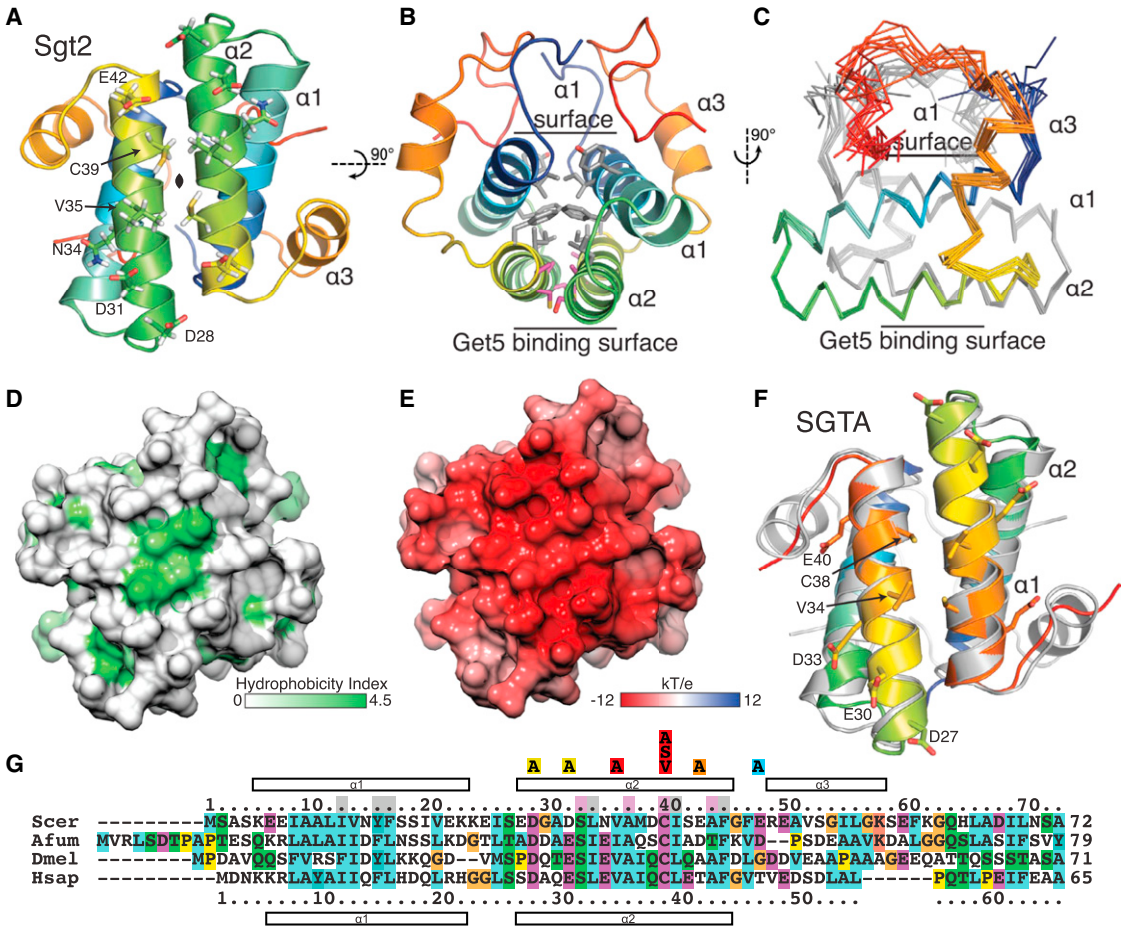

Figure 1. Atomic Structure of the Sgt2-N/SGTA-N Dimerization Domain

(A) Solution NMR structure of *S. cerevisiae* Sgt2-N oriented to show the Get5-binding surface. The cartoon diagram of a representative structure is color ramped from the N to C terminus (blue to red) for each subunit of the dimer. Conserved residues are shown as sticks with noncarbon atoms colored.

(B) Similar to (A), rotated 90° forward looking down the bundle axis. The locations of the Get5 binding and α1 surfaces are indicated. Interior small (magenta) and bulky (gray) residue side chains are highlighted as sticks, with hydrogens removed for clarity.

(C) Ribbon diagram of the overlaid ensemble of the ten lowest-energy NMR structures rotated 90° to the right relative to (B). One subunit is color ramped and one is in gray.

(D) Surface representation of the binding face highlighting exposed hydrophobicity. The surface is color ramped from 0 (gray) to 4.5 (green) on the Kyte-Doolittle hydrophobicity scale (Kyte and Doolittle, 1982).

(E) Surface representation of the binding face showing the surface charge. The surface is color ramped based on electrostatic potential colored from negative (red) to positive (blue).

(F) X-ray crystal structure of human SGTA-N aligned to Sgt2-N (gray), similar to (A).

(G) Sequence alignment of Sgt2-N homologs. The species are *S. cerevisiae* (Scr), *Aspergillus fumigatus* (Afum), *Drosophila melanogaster* (Dmel), and *Homo sapiens* (Hsap). Alignment and residue coloring are based on the ClustalX output (Larkin et al., 2007). Numbering and secondary structure (rectangles for helices) are indicated above or below the corresponding sequence. Mutations tested in Figure 3 are highlighted in the numbers colored based on effect.

See also Figure S1.

molecular replacement using the Get5-UBL solution structure. Three copies of Get5-UBL were present in the asymmetric unit (Figures 2B and S2B). They have an average root-mean-square deviation (rmsd) of 0.75 Å over main-chain atoms. Statistics for the solution structure calculations and crystallographic data collection and refinement are presented in Tables S1 and S2, respectively. The solution and crystal structures are very similar, with an average main-chain rmsd of 1.23 Å (Figure S2A) and with most variation in loops 1 and 5.

Although overall the structures from Get5 and UBL4A are similar, there are a few differences due to insertions (Figure S2C). Based on the structures and sequences of other animal homologs, Get5-UBL has a two-residue insertion around Pro84 in loop 1. Pro84 is *cis*, allowing for a tight turn, and there is no detectable *cis*-to-*trans* isomerization by NMR. There are two additional insertions in Get5-UBL, His113 in loop 3, and Ala141 that cause a short coil-like turn to extend at the end of loop 6. Despite these differences, the surface elements on the face of

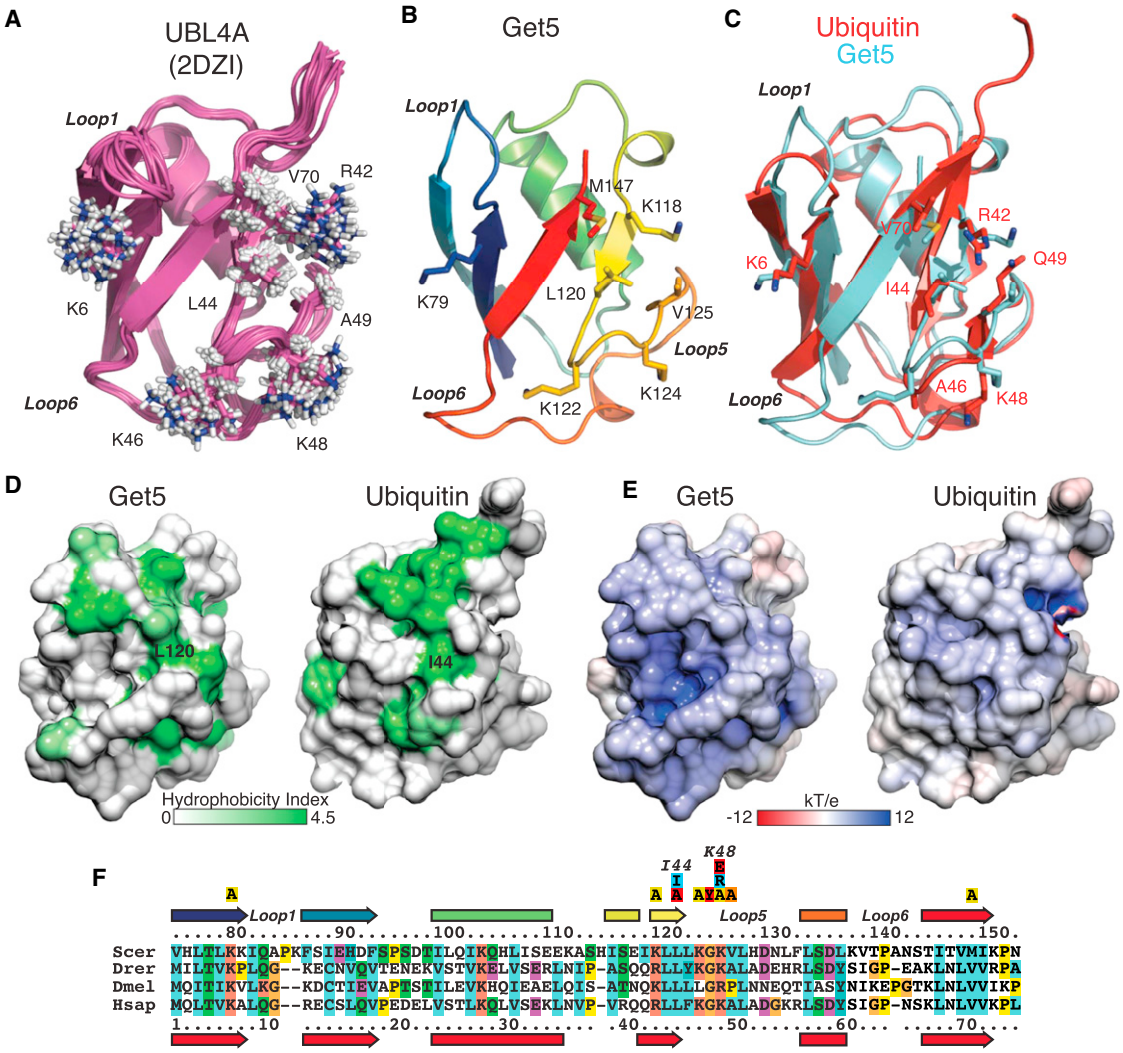

Figure 2. Atomic Structure of the Get5-UBL/UBL4A-UBL Domain

(A) Ribbon diagram of the human UBL4A-UBL domain solution structure (PDB ID: 1DZI). Residues equivalent to those tested in Figure 3 are highlighted as sticks in (A–C).

(B) X-ray crystal structure of the *S. cerevisiae* Get5-UBL domain. The cartoon of chain A is color ramped between termini.

(C) Overlay of a representative structure of ubiquitin (red, PDB ID: 1UBQ) is shown as a ribbon diagram with Get5-UBL (light blue).

(D) Surface representation highlighting the exposed hydrophobicity of Get5 and ubiquitin as in Figure 1D.

(E) Surface representation showing the surface electrostatic potential of Get5 and ubiquitin as in Figure 1E.

(F) Sequence alignment of Get5-UBL homologs. Sequences are displayed similarly to Figure 1G. In addition, beta-sheets are shown as arrows, and the residues equivalent to the important ubiquitin residues Ile44 and Lys48 are labeled. Drer, *Danio rerio*.

See also Figure S2.

the β sheet are conserved between Get5 and UBL4A (Figures 2A and 2B).

The UBL of Get5 and UBL4A have features that distinguish them from other UBLs with high homology to ubiquitin. UBLs occur either as independent units known as type I UBLs, which can be conjugated onto other proteins, or as type II UBLs, which are domains in larger proteins that frequently mediate binding to the proteasome (Jentsch and Pyrowolakis, 2000). Get5 falls into the latter class but does not associate with the 20S proteasome or polyubiquitin chains (Hu et al., 2006; Saeki et al., 2002). Therefore, one would expect that certain features distinguish Get5 homologs from other UBLs. When we compare Get5-UBL with ubiquitin, the two most significant structural differences are the conformations of loop 1 and loop 6 (Figure 2C). Get5 binds Sgt2 via its UBL through a hydrophobic patch formed by the conserved Leu120 (Chang et al., 2010; Chartron et al., 2011), which is equivalent to the conserved Ile44 of ubiquitin that forms the I44 patch (Hicke et al., 2005). In Get5, the conformations of loop 1 and loop 6 significantly reduce the size of the patch compared with ubiquitin (Figure 2D). Moreover, the

Sgt2	Get5	[NaCl] (mM)	K_d (nM)
wt[a]	wt	100	34
wt	wt	150	89
wt	wt	200	158
wt	wt	300	1317
wt	K79A	100	136
wt	K118A	100	191
wt	L120A	100	17100
wt	L120I	100	20
wt	K122A	100	463
wt	G123Y	100	17200
wt	K124A	100	181
wt	V125A	100	916
wt	M147A	100	497
wt	*wt*	100	15
D28A	*wt*	100	183
D31A	*wt*	100	175
V35A	*wt*	100	2060
C39A	*wt*	100	4320
C39S	*wt*	100	10600
C39V	*wt*	100	1470
E42A	*wt*	100	720
E47A	*wt*	100	16

[a]Italicized proteins were titrants

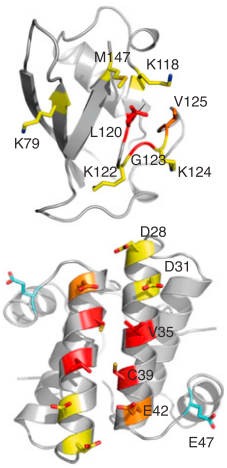

Figure 3. Importance of Conserved Residues of both Sgt2 and Get5 at the Putative Binding Interface by ITC

The table is a summary of the data obtained by ITC in which mutants were tested for binding affinity. Mutations tested are colored based on the loss of binding affinity (red, strong effect; orange, moderate effect; yellow, mild effect; blue, no significant effect). On the right, mutations are shown colored based on effect as sticks on a ribbon diagram of Get5-UBL (top) and Sgt2-N (bottom). See also Figure S3.

surface around the I44 patch has a positive charge for both proteins; however, it is significantly more pronounced in Get5 (Figure 2E).

Characterization of the Putative Interface between Sgt2-N and Get5-UBL

We previously demonstrated that only a single copy of Get5-UBL binds to dimeric Sgt2-N, and the double mutation L120A/K122A prevents complex formation (Chartron et al., 2011). We decided to probe the interaction further using isothermal titration calorimetry (ITC) of wild-type (WT) and mutant proteins (Figures 3 and S3). All variants behaved similarly to WT during purification (data not shown). Sgt2-N and Get5-UBL interact with 10^{-8} M affinity independently of which protein is used as a titrant. The Get5-UBL L120A mutation has a 1,000-fold lower binding affinity, consistent with the significance of this position in UBLs. The Get5-UBL L120I mutant bound Sgt2-N with affinity similar to that of the WT. This is surprising considering that a leucine at this position is completely conserved, in contrast to the isoleucine in most UBLs. Mutations of three other nearby hydrophobic residues that compose part of the hydrophobic patch (G123Y, V125A, and M147A) also significantly lowered the binding affinity.

The complementary surface charge of the two proteins suggests that a significant component of the interaction involves electrostatics. As expected for this type of binding, affinity drastically decreases as the salt concentration increases. Moreover, mutations of any of the lysines on this face of Get5-UBL (i.e., Lys79, Lys118, Lys122, or Lys124) to alanine reduce the binding affinity 5- to 10-fold. Interestingly, ubiquitin, which contains most of the residues tested, binds Sgt2-N with negligible affinity (data not shown).

We made reciprocal mutations to the conserved face of Sgt2-N and tested their binding to Get5-UBL (Figure 3). Similarly to Get5, mutation of the two exposed hydrophobic residues to alanine had the strongest effect with >100-fold lower affinity (V35A and C39A). The presence of the completely conserved cysteine was curious. We decided to make a series of typically minimal changes at this position to test for their effect on complex formation. A slightly bulkier hydrophobic side chain, C39V, resulted in a 100-fold lower affinity, whereas removing the sulfhydryl to a smaller amino acid, C39A, resulted in a nearly 300-fold lower affinity. The strongest effect was conversion of the sulfhydryl to the more-polar hydroxyl, C39S, which resulted in a ~700-fold lower affinity. Alanine mutations of the acidic residues that comprised the charged face had a similar effect on affinity compared with mutations of the basic residues of Get5-UBL. One exception was mutation of the peripheral Glu47, located at the beginning of α3, which had no effect on affinity.

Characterization of the Binding Kinetics of Sgt2-N and Get5-UBL

Multiple lines of evidence demonstrate complex formation between Get5 and Sgt2 (Chang et al., 2010; Chartron et al., 2011; Liou et al., 2007; Wang et al., 2010), and the complex formed by the minimal Get5-UBL and Sgt2-N domains appears stable by size exclusion chromatography. The ITC results suggest that the complex has high affinity; however, investigations using coimmunoprecipitation have shown variable amounts of Sgt2 or SGTA associated with the Get5/UBL4A partners. Although there are many possible reasons for this variability in stoichiometry in vivo, we hypothesized that fast binding kinetics could explain how coprecipitation might be dependent on experimental conditions. To measure the association and disassociation rate constants, we turned to surface plasmon resonance (SPR). In this experiment, polyhistidine-tagged Get5-UBL or Get5-UBL-C was immobilized and Sgt2-N was used as the analyte (Figure 4A). Get5-UBL-C includes the C-terminal dimerization domain of Get5, which is separated from the UBL domain by a flexible linker (Chartron et al., 2010). We previously demonstrated that the less-restrictive Get5-UBL-C dimer can bind two Sgt2-N domains (Chartron et al., 2011); therefore, we expected that each subunit would act independently. The proteins were well behaved on the chip, giving stable, concentration-dependent saturation (Figure 4B). The rapid saturation of response after analyte injection (<1 s) and then rapid reduction after the injection was stopped are indicative of fast on- and off-rates, consistent with our hypothesis.

We calculated the equilibrium dissociation constant by plotting response units as a function of Sgt2-N concentration after the response units reached equilibrium (Figures 4B–4D). For Get5-UBL-C, the plot fit to a K_d of 7.49×10^{-7} M. Compared with ITC, this is nearly two orders of magnitude lower affinity. Although the different techniques are not expected to give identical results, due to the different experimental conditions used, the relative results from mutants are consistent. We suspect that steric constraints based on interactions with the antibody affected the measured rates. This was seen when we used immobilized Get5-UBL, which is expected to bring the Sgt2

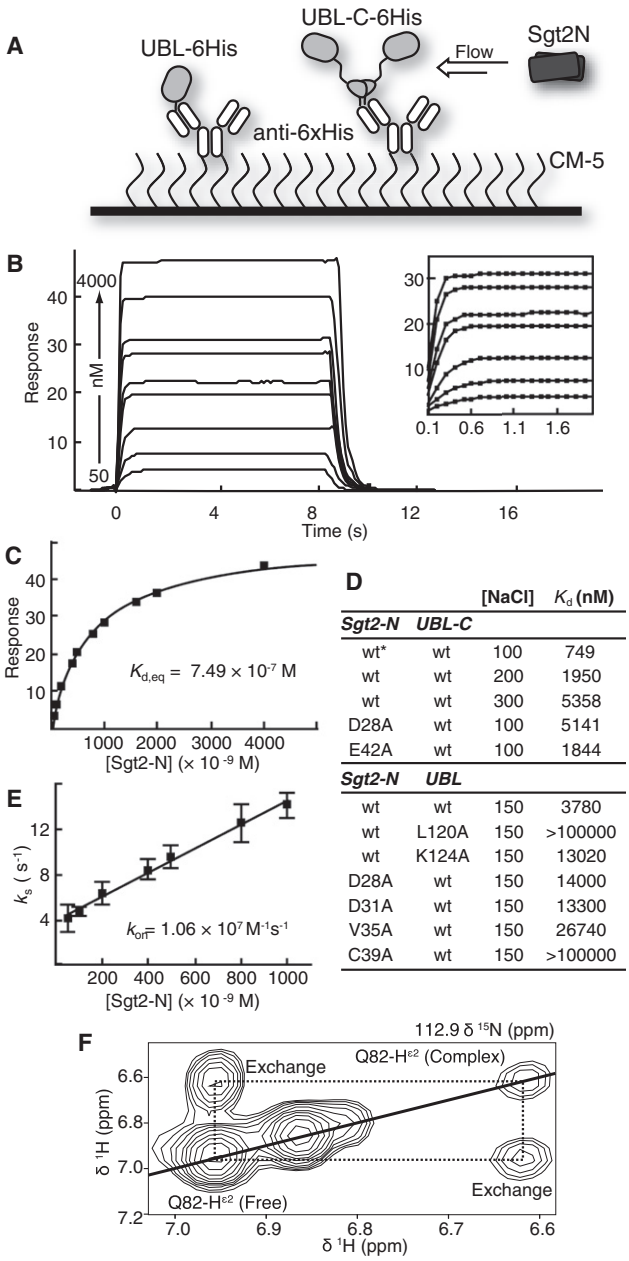

[NaCl]	K_d (nM)
Sgt2-N	***UBL-C***		
wt*	wt	100	749
wt	wt	200	1950
wt	wt	300	5358
D28A	wt	100	5141
E42A	wt	100	1844
Sgt2-N	***UBL***		
wt	wt	150	3780
wt	L120A	150	>100000
wt	K124A	150	13020
D28A	wt	150	14000
D31A	wt	150	13300
V35A	wt	150	26740
C39A	wt	150	>100000

Figure 4. Binding is Characterized by Rapid On- and Off-Rates Mediated by Electrostatics

(A) Scheme used for SPR analysis. Either His-tagged Get5-UBL (UBL-6His) or Get5-UBL-C (UBL-C-6His) was attached to an anti-6xHis antibody sparsely immobilized on a CM-5 chip. Sgt2-N was flowed over the chip at varying concentrations.

(B) Representative SPR experiment flowing varying concentrations of Sgt2-N over immobilized Get5-UBL-C. Inset: The first 2 s of the experiment, used to derive k_s for Figure 4E.

(C) Plot of equilibrium response units versus concentration of Sgt2-N for calculation of equilibrium K_d.

(D) Table of the effects of mutants and salt concentration on binding. An asterisk indicates the experiment performed in triplicate.

(E) Plot of the coefficient that fits k_s versus Sgt2-N concentration. The slope gives the association constant (k_a), and the Y intercept gives the dissociation rate (k_{off}). Error bars represent 1 SD.

binding face into closer proximity to the immobilizing antibody. This setup had consistently lower binding affinities; for example, WT binding was further reduced 5-fold to a K_d of 3.78 × 10^{-6} M. Mutants in Sgt2-N or Get5-UBL showed similar changes in binding affinity compared with ITC. The charged mutants Get5-UBL K124A, Sgt2-N D28A, and Sgt2-N D31A all had similar affinities that were on the order of 3- to 4-fold weaker than that of the WT protein. Also, residues in the hydrophobic interface had the strongest effect, reducing the affinity of Get5-UBL L120A or Sgt2-N C39A to below what could be accurately determined in this experimental setup.

The importance of charge complementarity is consistent with two preformed interfaces that are electrostatically steered toward complex formation. These types of protein interactions are known to have fast binding kinetics (Sheinerman et al., 2000). Here, we used the association phase of the SPR data to determine a k_{on} of 1.06 × 10^7 M^{-1} s^{-1} and a dissociation rate constant of ~4 s^{-1} (Figure 4E). The dissociation rate constant could be independently estimated from the equilibrium K_d and k_{on} values, which gives an approximate k_{off} of 7.9 s^{-1}. Consistent with both the electrostatic mechanism and the ITC data, increasing the salt concentration from 100 to 300 mM salt resulted in nearly an order of magnitude change in K_d (Figure 4D). All of these data point to a highly specific interface that has rapid on- and off-rates.

For independent verification of the kinetics, we measured the exchange rates by NMR using exchange spectroscopy (EXSY; Perrin and Dwyer, 1990). A 2:1 ratio of ^{15}N-labeled Get5-UBL to unlabeled Sgt2-N homodimer was prepared, allowing detection of approximately equimolar free and complex forms of Get5-UBL. The complex dissociated and reformed within the timescale of the experiment (mixing time, τ_m, = 60 or 120 ms). As a result, exchange cross peaks were observed for every proton that had a change in chemical shift between the two states of Get5-UBL (Figures 4F and S4A). The side-chain amide protons of Gln82 and the main-chain amide protons of Val125, Asn129, Met147, Ile148, and Lys149 produced exchange peaks with enough resolution for volume integration. The magnitudes of these peaks were used to calculate the exchange rates (Figure S4B). Overall exchange rates of 7.5 ± 2.5 s^{-1} (τ_m = 60 ms) or 5.7 ± 2.4 s^{-1} (τ_m = 120 ms) were obtained and represent $k_{off,NMR}$. Using the ITC-derived K_d of 34 nM, $k_{on,NMR}$ is ~2.0 × 10^8 M^{-1} s^{-1}, which is 20-fold faster than that measured by SPR. Because the solution and immobilized Get5 off-rates are similar, the lower binding affinity seen by Get5 immobilization in the SPR experiment is from a slower k_{on}. Finally, a high-affinity complex with fast kinetics is consistent the single peak seen by size exclusion chromatography (Stevens, 1989).

Structure of the Sgt2-N and Get5-UBL Complex

Compared with the proteins alone, the NMR spectra of the Sgt2-N/Get5-UBL complex have a dramatic reduction in

(F) Plot of a ^{15}N plane from an EXSY-HSQC spectrum showing a side-chain amide proton of Gln82 in free or complex Get5-UBL. The cross peaks indicate exchange between the two states within the timescale of the experiment. Similar plots for main-chain protons are provided in Figure S4A.

See also Figure S4.

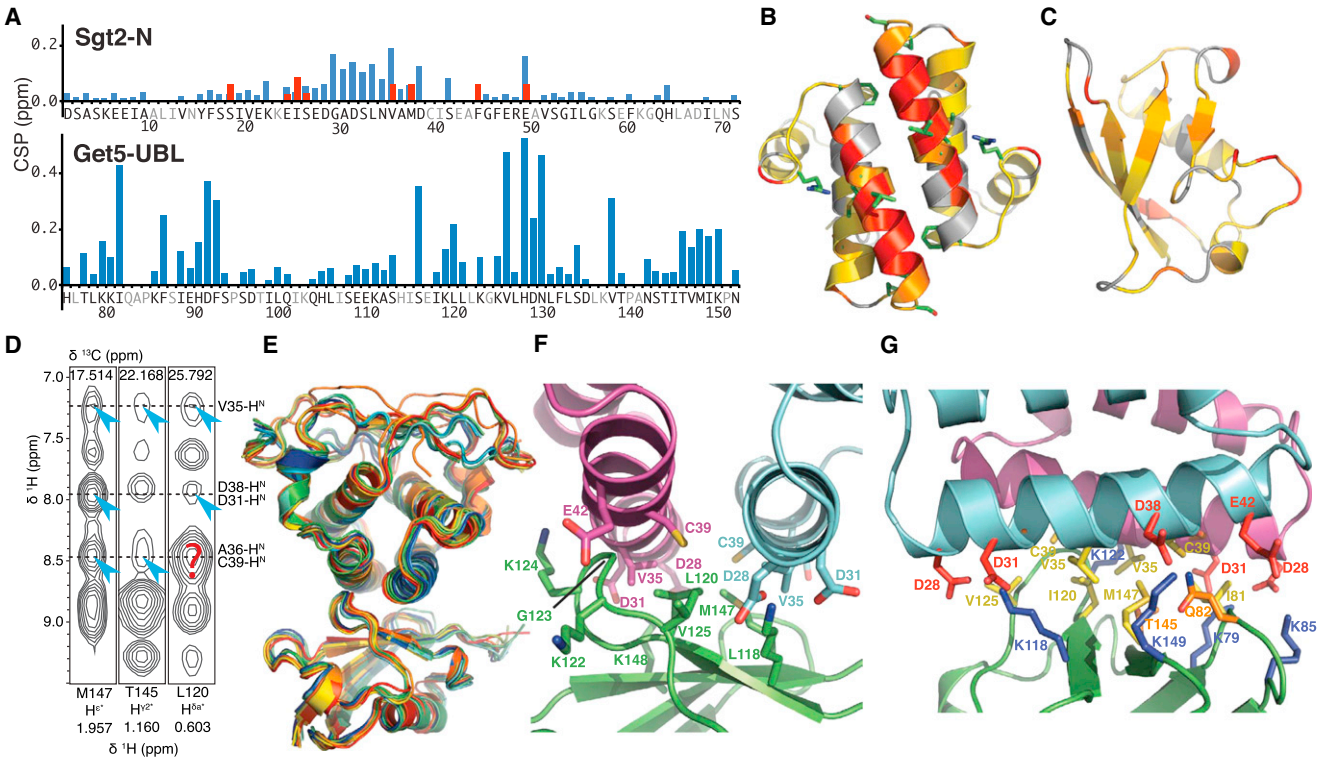

Figure 5. Solution Structure of the Sgt2-N/Get5-UBL Complex

(A) Plots of the change in chemical shifts of the ^{1}H-^{15}N HSQC as a combined CSP upon complex formation for each residue at 25°C. Changes for residues in gray could not be accurately determined due to cross-peak overlap. For Sgt2-N, several residues were split into two peaks, breaking the symmetry. These are indicated in red.

(B) Cartoon representation of Sgt2-N illustrating regions of chemical shift change between the free protein and the complex (cyan). Coloring is based on values from (A). Residues are color ramped from the smallest (yellow) to the largest (red) CSP. Residues that could not be measured are shown in gray. Residues with split chemical shifts upon complex formation are shown as green sticks.

(C) Cartoon representation of Get5-UBL, similar to (B).

(D) Representative intermolecular NOEs from a ^{13}C-edited NOESY-HSQC spectrum at 37°C constrained to be <6 Å away during docking. Peaks identified as intermolecular are highlighted by a blue arrowhead and labeled. The red question mark represents a peak that is unresolvable from an expected intramolecular NOE.

(E) Overlay of the ten best-scored models obtained after NOE-, AIR-, and RDC-driven docking.

(F and G) Two views of the binding interface. In (F), residues determined to interact by ITC are highlighted as sticks. In (G), residues at the interface are drawn as sticks with the following color scheme: blue, positive; red, negative; orange, polar; yellow, hydrophobic.

See also Figure S5.

resolution. This is a result of peak broadening due to both slower tumbling and the fast kinetics of complex formation and dissociation. Therefore, instead of generating a uniformly $^{13}C/^{15}N$-labeled sample of 235 residues, we opted to investigate two asymmetrically labeled complexes to reduce the amount of chemical shift overlap. Chemical shift perturbations (CSPs) on the two-dimensional (2D) ^{1}H-^{15}N heteronuclear single quantum coherence (HSQC) spectra were examined for both proteins (Figure 5A). On Sgt2, the most drastic CSPs occurred at the Get5 binding surface, with very little change occurring in the rest of the protein (Figure 5B). Binding of a single Get5-UBL is anticipated to break the symmetry of Sgt2-N, and indeed several residues on the Get5 binding surface split into two cross peaks with reduced peak height (Figures 5A and S5A). Residues without perturbation maintained a single cross peak, indicating that symmetry remained away from the binding site. The Get5-UBL domain was more broadly affected by binding to Sgt2-N, but the most intense CSPs occurred at Ile81 and the loop consisting of residues 123–129, including Gly123 and Val125.

Inspection of NOE spectroscopy (NOESY) spectra failed to conclusively identify enough new cross peaks resulting from intermolecular contacts to determine the structure by NOE distance restraints alone. This is not surprising, given the presumed interface. Electrostatic interactions between a glutamate or aspartate and a lysine yield weak proton NOE cross-peaks. Additionally, the expected hydrophobic interactions occur in crowded regions of the spectra. We proceeded to determine the individual solution structures of Sgt2-N and Get5-UBL as they are in complex. Data collection for the full assignments of the proteins in complex was performed at 37°C, which reduced the severity of line-broadening effects.

This had the additional effect of averaging the two states of Sgt2-N; therefore, we treated Sgt2-N as symmetric in these calculations.

Overall, the structures of Sgt2-N and Get5-UBL while in complex are not significantly different from the free solution structures (Figures S5B and S5C). A few intermolecular NOEs could be identified and were used in the calculation of the complex structure (Figure 5D). In the absence of substantial numbers of NOE-derived distance restraints, the structures of complexes can be determined by molecular docking driven by other experimental data introduced as ambiguous interaction restraints (AIRs; Dominguez et al., 2003). We defined 14 AIRs using the CSP and mutagenesis data, the details of which are provided in the Extended Experimental Procedures. Moreover, we collected residual dipolar couplings (RDCs) that restricted rotational freedom between the models during docking. We performed docking between the two separate complex structures to generate a full model of Sgt2-N and Get5-UBL (Figure 5E). Statistics for the structure calculation of each component, as well as the complex, are provided in Tables S3 and S4.

The experimentally restrained docking returns a well-converged structure in which the predicted binding faces interact (Figure 5E). All of the residues that were identified to be involved experimentally are found at the interface (Figure 5F). The interface is comprised of the hydrophobic patch on Get5-UBL (Ile81, Leu120, Val125, Gly143, and Met147) that docks against the reciprocal patch that contains two each of Cys39 and Val35 from the Sgt2-N dimer (Figure 5G). Additionally, Thr145 packs against one copy of Val35. The conserved lysines 79, 85, 118, 122, and 149 all make electrostatic contacts to the charged face of Sgt2-N (two each of Asp28, Asp31, Asp38, and Glu42).

The Complex Is a Unique UBD/UBL Interaction

Ubiquitin and UBL domains are abundant in cells and all share common features (Winget and Mayor, 2010). Perhaps more abundant are the different UBD motifs found in a wide variety of frameworks (Hicke et al., 2005; Husnjak and Dikic, 2012). The combinatorial use of UBLs and UBDs results in a wide diversity of interactions that are utilized in many different contexts. The complex between Sgt2 and Get5 introduces a novel interaction.

As is typical of the most commonly observed UBD interactions, Sgt2-N binds at the face that contains the I44 patch (Figures 6A and 6B). In contrast to other UBDs, Sgt2 uses a symmetrical dimer interface to interact with its UBL. The only other example of a UBD dimer is the swapped CUE motif found in Vps9, which binds similarly to other CUE domains (Figure 6B; PDB ID: 2P3Q; Prag et al., 2003). Most of the other characterized UBDs bind primarily with a single polypeptide. A comparison of UBD binding interfaces reveals that Sgt2 buries a relatively large surface area (682.8Å^2; Figures 6A and 6B). The next closest interface for a yeast UBD is that of Ufd2 bound to the UBL of Rad23, which has an interface of 614.3Å^2 (Hänzelmann et al., 2010).

Most of the I44 patch-binding UBDs use α-helical motifs, as does Sgt2. These proteins interact with similar groups of residues on their respective UBLs (Figures 6C and 6D). UBLs have a number of conserved residues around the I44 patch. For ubiquitin, these include Leu8, Arg42, Ile44, Gly47, His68, and Val70. These interactions are conserved on Get5 in the interface with Sgt2 (Ile81, Lys118, Leu120, Gly123, Thr145, and Met147). Most of these residues are similar in nature to the canonical residues, except for Thr145, which is a histidine in most UBLs.

Of the Sgt2/Get5 interactions, the most interesting involve residues that are unique in the interface relative to all other UBLs (Figures 6C and 6D). Four residues fit this description. The most provocative, the highly conserved Ile44 of ubiquitin, is a leucine in all Get5 homologs. Surprisingly, mutating this to isoleucine had no effect on binding affinity (Figure 3). The second is Gln82 in Get5, which forms a conserved hydrogen-bond network with negative charges on Sgt2. In ubiquitin, this residue is a threonine that likely cannot contribute to a similar network, and in fact is pointed away from the I44 patch. Next is Lys122, a positive charge that is conserved in Get5 homologs adjacent to the I44 patch but is missing in other UBLs. This lysine forms salt bridges with the conserved Asp28 and Asp31 on Sgt2. In ubiquitin, this position is an alanine whose side chain is pointed away from the interface. The final residue is Thr145, whose equivalent in ubiquitin is a histidine (His68). In UBL4A, the position is an asparagine, a more polar residue. For ubiquitin, His68 is typically described as a component of the hydrophobic pocket lining the edge of the I44 patch. For the Get5/Sgt2 complex, the smaller threonine is likely required to accommodate the tight interface.

DISCUSSION

The biogenesis of TA membrane proteins requires sorting in the cytoplasm, followed by targeting to the membrane and then subsequent insertion into the bilayer. For TAs destined for the ER, the conserved GET pathway governs this process. Sgt2 and Get5 are members of the so-called yeast TRC, which includes Get4 and HSPs. This complex is responsible for binding and then sorting of ER-destined TAs to the targeting factor, Get3 (Wang et al., 2010). Sgt2 contains three domains (Figure 7A). The C-terminal domain binds hydrophobic peptides with varying affinities. Mitochondrial TA proteins are typically less polar compared with ER-destined substrates, and it is thought that this feature allows Sgt2 to selectively bind the latter with higher affinity (Wang et al., 2010). The central domain contains three TPR repeats that bind multiple classes of HSP proteins whose structure was recently solved (Chartron et al., 2011). At the N terminus is a homodimerization domain whose structure is reported here. In solution, Sgt2 forms an extended dimeric complex with the C-terminal domain moving freely at the end. Get5 forms an obligate heterotetramer with Get4 (Figure 7A). Get5 contains three domains: (1) an N-terminal domain, which wraps around Get4 to form the heterodimer interface (Chang et al., 2010; Chartron et al., 2010); (2) a C-terminal domain, which forms a small, stable dimerization motif whose structure was also recently solved (Chartron et al., 2012b); and (3) the central domain, which is a novel UBL domain whose structure we report here. The Get4/Get5 complex is also extended in solution (Chartron et al., 2010, 2011).

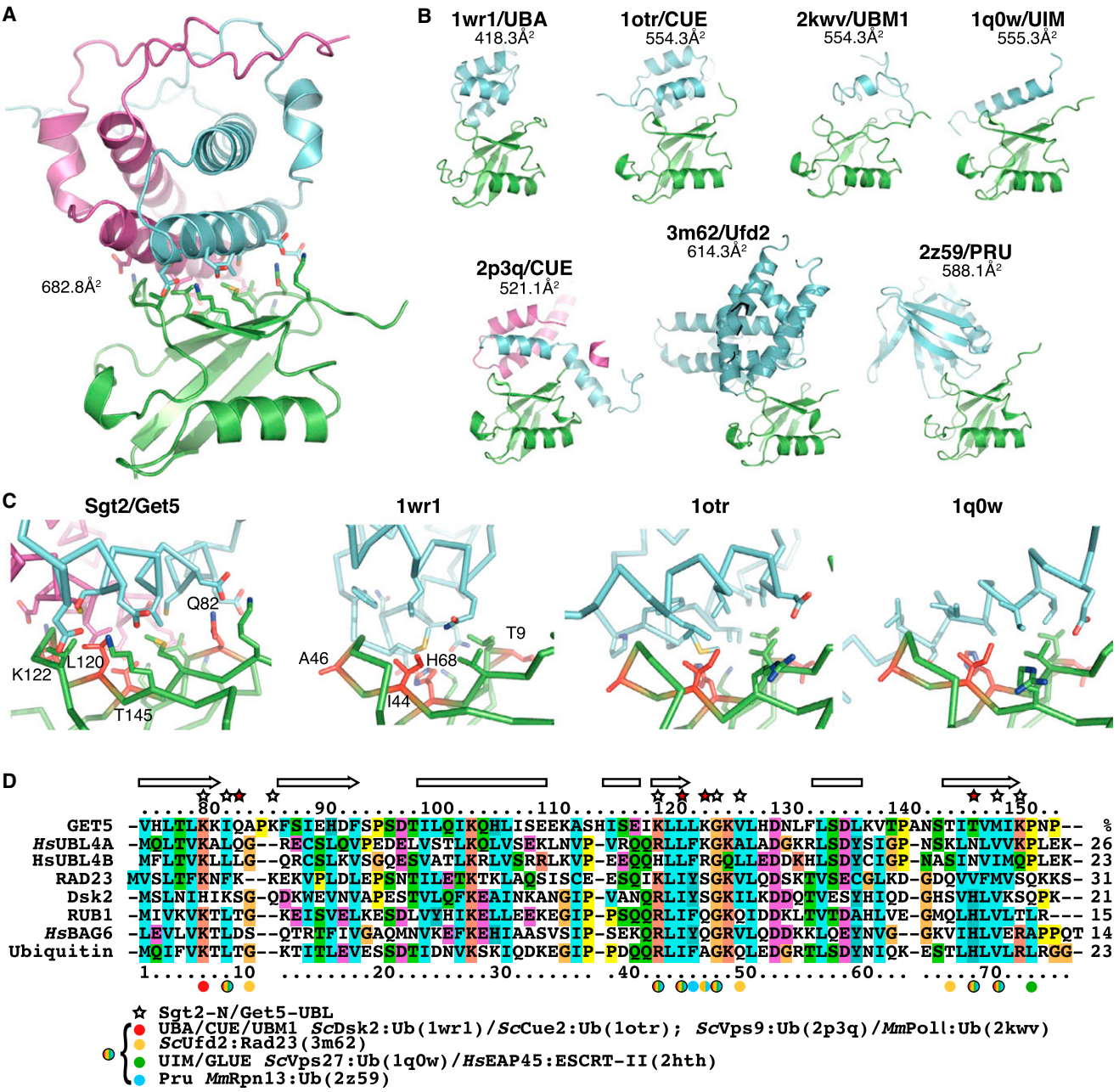

Figure 6. The Sgt2-N/Get5-UBL Complex Is a Unique UBD/UBL Interface

(A) View of the complex shown as a cartoon diagram (Sgt2-N in cyan and purple, Get5-UBL in green). Residues involved in the interface are drawn as sticks. The interface surface area, determined using the Protein Interfaces, Surfaces, and Assemblies (PISA) tool, is indicated (Krissinel and Henrick, 2007).

(B) Representative structures of various UBD (cyan)/UBL (green) complexes that interact with the I44 patch, shown as a cartoon aligned to the Get5-UBL in (A). Each structure is labeled with its PDB ID and the UBD group that is represented (reviewed in Hicke et al., 2005; Husnjak and Dikic, 2012). Proteins are named in (D). Interface surface areas are indicated.

(C) View of the binding interface of representative helical UBDs. Residues at the interface are shown as sticks in (D). Get5-UBL residues Q83, L120, K122, and T145 are colored red. Equivalent residues in other structures are also highlighted.

(D) Sequence alignment of *S. cerevisiae* UBL domains with human UBL4A, UBL4B, and BAG6 UBLs included. Alignment is similar to that in Figure 1C. Numbers at the end of the sequence are percent identity to Get5. Residues that interact with various UBDs are highlighted based on the legend. Stars filled with red are highlighted in (C).

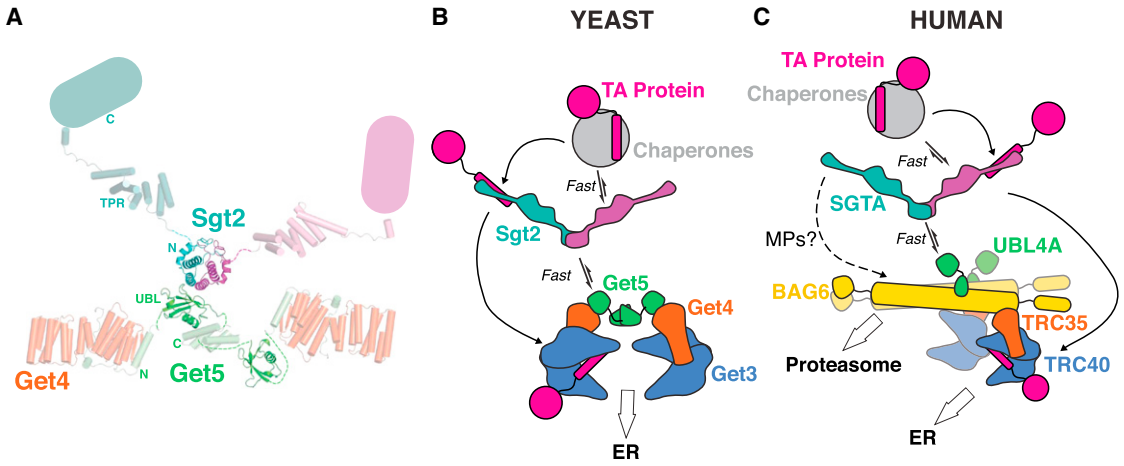

Figure 7. Model for the Role of the Sgt2/Get5 Complex

(A) Composite model of the Sgt2/Get4/Get5 complex based on all available structural data. In the center is the complex reported here. Sgt2 is an extended dimer (cyan and magenta). The TPR domains extend away from each other (PDB ID: 3SZ7). The C-terminal domains, represented as rounded rectangles, are flexible. The Get4/Get5 complex is an extended homodimer mediated by the Get5-C domain (PDB ID: 3VEJ). Get4 forms a complex with the Get5-N domain (PDB ID: 3LKU).

(B) Model of the TRC complex in the GET pathway. Chaperones binding hydrophobic proteins rapidly bind and dissociate from the TPR domain of Sgt2. The C-terminal domain of Sgt2 binds to ER-destined TA proteins. Sgt2 is rapidly binding and dissociating from Get4/Get5, which binds to Get3.The TA protein is then transferred from Sgt2 to Get3.

(C) Model of the mammalian TRC pathway. Chaperones and SGTA act analogously to the yeast system in (B). SGTA rapidly binds to and dissociates from UBL4A. The BAG6 complex then sorts substrates between the TA targeting pathway, mediated by TRC35 and TRC40 and the proteasome.

The initial identification of Get4 and Get5 as bona fide members of the GET pathway did not reveal the connection to Sgt2 (Jonikas et al., 2009). In hindsight, this is surprising, because previous biochemical and genetic links had been reported (Liou et al., 2007). Subsequent studies clearly linked the N-terminal dimerization domain of Sgt2 to the UBL domain of Get5, solidifying the role of Sgt2 in TA targeting (Battle et al., 2010; Chang et al., 2010; Chartron et al., 2011; Wang et al., 2010). We previously demonstrated that although the complex thus formed was stable enough for copurification, the interface was sensitive to mutation (Chartron et al., 2011, 2012b). The structures reveal a strong electrostatic component to the interface between Get5 and Sgt2, which results in a complex with fast on- and off-rates.

The affinity of Sgt2 to Get5 is remarkably high (Figure 3). In the cell, every Get4/Get5 heterotetramer will, on average, be bound by an Sgt2, and as one falls off, another one quickly replaces it, consistent with experimental results (Wang et al., 2010). Our previous work demonstrated that only a single Sgt2 dimer could bind to the Get4/Get5 heterotetramer at one time (Chartron et al., 2012b); therefore, Get5 has two potential binding sites for Sgt2s that are rapidly sampling. This makes sense in a model for TA targeting (Figure 7B), because a Get3/Get4/Get5 complex would be stable in the cytoplasm. This complex would screen Sgt2 proteins, over multiple rounds, to find one that stably binds an ER-destined TA protein. This interaction would lead to a handoff of the TA to Get3, which would then be released from Get4 to find its ER receptors. How Sgt2 finds TA proteins is a matter of conjecture. The simplest model is that it captures free TAs in the cytoplasm; however, it remains seductive to imagine that the highly abundant HSPs provide at least one route into the pathway. In that context, Sgt2 would bind HSPs transiently, allowing for multiple rounds of binding to find appropriate substrates. Once a TA protein is bound, it becomes be a stable complex that can be found by Get4/Get5.

In metazoans, the picture becomes more complicated (Figure 7C). In addition to homologs for the yeast GET proteins, TA targeting includes a large multidomain protein called BAG6. BAG6 contains an N-terminal UBL domain that has features characteristic of typical UBLs (Figure 6D) and a C-terminal BAG domain. It is linked to TA targeting by forming a stable complex with TRC35 and UBL4A (Mariappan et al., 2010). TRC35 and UBL4A lack the features necessary for direct complex formation in yeast (Chartron et al., 2010, 2012a) and it is likely that they both bind BAG6 directly. The first structure solved from this complex is the UBL domain from UBL4A (PDB ID: 2DZI), which has not been described in the literature. Although it has yet to be experimentally demonstrated, it seems very likely that SGTA performs a similar role in TA targeting to its yeast counterpart (Figure 7C). The structure of the dimerization motif of SGTA supports this, because it is a highly conserved domain, like UBL4A-UBL, with all of the features that are important for heterodimer formation. BAG6 has been demonstrated to be a dimer and to form a complex with SGTA via the UBL domain of UBL4A (Y. Ye, personal communication). This then would mirror all of the components of the yeast system, including two each of SGTA, UBL4A, and TRC35 (Figure 7C).

In mammalian cells, the BAG6 complex is linked to the degradation of mislocalized membrane proteins and dislocated ER products (Hessa et al., 2011; Wang et al., 2011). TA proteins can be redirected to the degradation pathway, suggesting that the two pathways intersect (Hessa et al., 2011). SGTA has now

been shown to be an important component for targeted degradation of ERAD substrates that transiently bind hydrophobic membrane proteins prior to handoff to BAG6 (Figure 7C; Y. Ye, personal communication). This additional role would also benefit from rapid sampling of SGTA to the BAG6 complex, raising the possibility that in yeast, Sgt2 could have multiple roles as well.

Where proteins are linked to degradation pathways, it seems plausible that multiple UBLs divergently evolve to fill more specific roles. This is clear for the BAG6-UBL, which has all of the features of UBLs involved in degradation and is critical for targeting to the proteasome (Hessa et al., 2011; Wang et al., 2011). The Get5/UBL4A UBL represents a unique class of UBLs with features that clearly distinguish them from other UBLs (Figure 6). In fact, when the conserved histidine of the BAG6-UBL is converted to an asparagine, it completely loses its ability to bind to standard UBDs (Y. Ye, personal communication). A similar effect is not seen when the conserved Leu120 is replaced by an isoleucine, although this could be a change to prevent other UBDs from binding Get5.

Sgt2 and SGTA are UBDs that have very specific binding partners. An interface dominated by electrostatics is unique among UBL/UBD complexes. This presumably allows high-affinity, rapid binding while strongly rejecting unfavorable interactions with other UBLs and UBDs. One interesting side note is that in mammals, both UBL4A and SGTA have tissue-specific isoforms: Ubl4B and SGTB (Tobaben et al., 2003; Yang et al., 2007). Although SGTA and SGTB have similar conserved sequence elements, UBL4B is missing a number of the residues that likely form the SGTA/UBL4A interface (Figure 6D). This suggests that it may have lower affinity or perhaps an unknown UBD.

In this report, we demonstrate a conserved UBD/UBL interaction that is critical for TA targeting. The complex is in a dynamic equilibrium that allows for rapid sampling of the various components. This attribute is likely essential for the various roles that Sgt2 homologs must play. This work opens the door to understanding the steps of target selection and discrimination that are required for a regulated process. The finer details of the process of TA targeting continue to be resolved at a rapid pace; however, each new insight leads to unexpected elaborations. With the recent link to regulated proteolysis, TA targeting is becoming part of the greater picture of homeostasis in the cell.

EXPERIMENTAL PROCEDURES

Solution NMR Structure Determination

Sgt2-N and Get5-UBL were overexpressed and purified from *Escherichia coli*. Chemical shift assignments were made using uniformly $^{13}C/^{15}N$-labeled samples. Data were collected on a Varian Inova 600 MHz spectrometer with a triple-resonance probe or a Bruker Avance 800 MHz with a TCI cryoprobe. Structures were calculated using NOE-derived distance restraints.

Double-labeled proteins were mixed with excesses of natural abundance protein. The asymmetrically labeled complexes were then purified by size exclusion chromatography. Chemical shifts were assigned and structures were calculated separately for each protein in the complex. CSP and mutagenesis data were used to define AIRs that were used along with 14 intermolecular NOE distance restraints and RDCs to calculate the complete structure of the complex (Dominguez et al., 2003). Details of the solution NMR experiments are provided in Extended Experimental Procedures.

Determination of SGTA-N and Get5-UBL Crystal Structures

Human SGTA-N and UBL4A-UBL were coexpressed in *E. coli* and purified by affinity and size exclusion chromatography. All crystallizations were performed by the vapor diffusion technique. Diffraction data were collected at beamline 12-2 at the Stanford Synchrotron Radiation Lightsource (SSRL). Phases were recovered by molecular replacement using the solution NMR structures presented here. Additional details regarding crystal growth, data collection, and model refinement are provided in Extended Experimental Procedures.

ITC

Data were collected with a MicroCal iTC-200 calorimeter. Details of the sample preparation are provided in Extended Experimental Procedures. Proteins in the sample cell were at 30–100 μM, and proteins in the injection syringe were concentrated to 800–1,000 μM. For each experiment, an initial injection of 0.4 μl was followed by 19 injections of 2 μl each. The cell was allowed to equilibrate for 120 s between titrations. Data were processed using Origin v7.0 (OriginLab) software with a single-site model.

SPR

Sample and running conditions are described in Extended Experimental Procedures. Data were collected using a Biacore T-100 system upgraded to T-200 sensitivity (GE Healthcare). Mouse anti-pentahistidine antibody (QIAGEN) was covalently linked to a CM5 dextran chip using standard amide coupling chemistry. Hexahistidine-tagged Get5-UBL (WT or mutants) or Get5-UBL-C were then immobilized. An equilibrium binding analysis was performed using BIAevaluation software (GE Healthcare). A kinetic analysis between WT Sgt2-N and Get5-UBL was performed using Kaleidagraph (Synergy Software). The slope values k_s at each concentration were determined by linear regression fitting of the association phase to the integrated first-order rate equation. Values of k_s were plotted against concentration, and the association rate k_{on} was determined from the linear fit to Equation 1:

$$k_s = k_{on} \times [\text{Sgt2-N}] + k_{off}. \quad \text{(Equation 1)}$$

This fit results in a k_{off} of 3.9 s^{-1}, but because k_{off} may not accurately be determined by this method (Karlsson et al., 1991), we additionally estimated it using the equilibrium dissociation constant as the ratio of k_{off} to k_{on}.

ACCESSION NUMBERS

The atomic coordinates and structure factors or NMR restraints have been deposited in the RCSB Protein Data Bank (http://www.pdb.org) with PDB ID codes 2LXB, 4GOD, 4GOE, 4GOF, 2LXA, 4GOC, and 2LXC for the Sgt2-N (NMR), three SGTA-N (X-ray), Get5-UBL (NMR), Get5-UBL (X-ray), and Get5-UBL/Sgt2-N structures, respectively. The chemical shifts have been deposited in the Biological Magnetic Resonance Bank (http://www.bmrb.wisc.edu/) with accession numbers 18669, 18670, and 18671 for Get5-UBL, Sgt2-N, and Get5-UBL/Sgt2-N, respectively.

SUPPLEMENTAL INFORMATION

Supplemental Information includes Extended Experimental Procedures, five figures, and four tables and can be found with this article online at http://dx.doi.org/10.1016/j.celrep.2012.10.010.

LICENSING INFORMATION

ACKNOWLEDGMENTS

We thank Yihong Ye (National Institutes of Health [NIH], Bethesda, MD) for valuable discussion and for providing unpublished data. We thank Shu-Ou Shan, Douglas Rees, Axel Müller, Meera Rao, Christian Suloway, and Michael

Rome for critical readings of the manuscript. We thank members of the Clemons laboratory for support and useful discussions. We thank Graeme Card, Ana Gonzalez, and Michael Soltice for help with data collection at SSRL beamline 12-2; Robert Peterson and Juli Feigon for use of the 800 MHz NMR spectrometer at the University of California, Los Angeles; Jost Vielmetter, Harry Gristick, Claude Rogers, and Abigail Pulsipher for assistance with SPR and ITC experiments; and Gordon and Betty Moore for support at the Molecular Observatory at Caltech. Operations at the SSRL are supported by the U.S. Department of Energy and the NIH. W.M.C. is supported by NIH grant R01GM097572.

Received: July 20, 2012
Revised: September 25, 2012
Accepted: October 8, 2012
Published: November 8, 2012

REFERENCES

Battle, A., Jonikas, M.C., Walter, P., Weissman, J.S., and Koller, D. (2010). Automated identification of pathways from quantitative genetic interaction data. Mol. Syst. Biol. *6*, 379.

Bozkurt, G., Wild, K., Amlacher, S., Hurt, E., Dobberstein, B., and Sinning, I. (2010). The structure of Get4 reveals an alpha-solenoid fold adapted for multiple interactions in tail-anchored protein biogenesis. FEBS Lett. *584*, 1509–1514.

Chang, Y.-W., Chuang, Y.-C., Ho, Y.-C., Cheng, M.-Y., Sun, Y.-J., Hsiao, C.-D., and Wang, C. (2010). Crystal structure of Get4-Get5 complex and its interactions with Sgt2, Get3, and Ydj1. J. Biol. Chem. *285*, 9962–9970.

Chartron, J.W., Suloway, C.J.M., Zaslaver, M., and Clemons, W.M., Jr. (2010). Structural characterization of the Get4/Get5 complex and its interaction with Get3. Proc. Natl. Acad. Sci. USA *107*, 12127–12132.

Chartron, J.W., Gonzalez, G.M., and Clemons, W.M., Jr. (2011). A structural model of the Sgt2 protein and its interactions with chaperones and the Get4/Get5 complex. J. Biol. Chem. *286*, 34325–34334.

Chartron, J.W., Clemons, W.M., Jr., and Suloway, C.J. (2012a). The complex process of GETting tail-anchored membrane proteins to the ER. Curr. Opin. Struct. Biol. *22*, 217–224.

Chartron, J.W., VanderVelde, D.G., Rao, M., and Clemons, W.M., Jr. (2012b). Get5 carboxyl-terminal domain is a novel dimerization motif that tethers an extended Get4/Get5 complex. J. Biol. Chem. *287*, 8310–8317.

Costanzo, M., Baryshnikova, A., Bellay, J., Kim, Y., Spear, E.D., Sevier, C.S., Ding, H., Koh, J.L.Y., Toufighi, K., Mostafavi, S., et al. (2010). The genetic landscape of a cell. Science *327*, 425–431.

Denic, V. (2012). A portrait of the GET pathway as a surprisingly complicated young man. Trends Biochem. Sci. *37*, 411–417.

Dominguez, C., Boelens, R., and Bonvin, A.M.J.J. (2003). HADDOCK: a protein-protein docking approach based on biochemical or biophysical information. J. Am. Chem. Soc. *125*, 1731–1737.

Dutta, S., and Tan, Y.-J. (2008). Structural and functional characterization of human SGT and its interaction with Vpu of the human immunodeficiency virus type 1. Biochemistry *47*, 10123–10131.

Hänzelmann, P., Stingele, J., Hofmann, K., Schindelin, H., and Raasi, S. (2010). The yeast E4 ubiquitin ligase Ufd2 interacts with the ubiquitin-like domains of Rad23 and Dsk2 via a novel and distinct ubiquitin-like binding domain. J. Biol. Chem. *285*, 20390–20398.

Hegde, R.S., and Keenan, R.J. (2011). Tail-anchored membrane protein insertion into the endoplasmic reticulum. Nat. Rev. Mol. Cell Biol. *12*, 787–798.

Hessa, T., Sharma, A., Mariappan, M., Eshleman, H.D., Gutierrez, E., and Hegde, R.S. (2011). Protein targeting and degradation are coupled for elimination of mislocalized proteins. Nature *475*, 394–397.

Hicke, L., Schubert, H.L., and Hill, C.P. (2005). Ubiquitin-binding domains. Nat. Rev. Mol. Cell Biol. *6*, 610–621.

Hu, Z., Potthoff, B., Hollenberg, C.P., and Ramezani-Rad, M. (2006). Mdy2, a ubiquitin-like (UBL)-domain protein, is required for efficient mating in Saccharomyces cerevisiae. J. Cell Sci. *119*, 326–338.

Husnjak, K., and Dikic, I. (2012). Ubiquitin-binding proteins: decoders of ubiquitin-mediated cellular functions. Annu. Rev. Biochem. *81*, 291–322.

Jentsch, S., and Pyrowolakis, G. (2000). Ubiquitin and its kin: how close are the family ties? Trends Cell Biol. *10*, 335–342.

Jonikas, M.C., Collins, S.R., Denic, V., Oh, E., Quan, E.M., Schmid, V., Weibezahn, J., Schwappach, B., Walter, P., Weissman, J.S., and Schuldiner, M. (2009). Comprehensive characterization of genes required for protein folding in the endoplasmic reticulum. Science *323*, 1693–1697.

Karlsson, R., Michaelsson, A., and Mattsson, L. (1991). Kinetic analysis of monoclonal antibody-antigen interactions with a new biosensor based analytical system. J. Immunol. Methods *145*, 229–240.

Kohl, C., Tessarz, P., von der Malsburg, K., Zahn, R., Bukau, B., and Mogk, A. (2011). Cooperative and independent activities of Sgt2 and Get5 in the targeting of tail-anchored proteins. Biol. Chem. *392*, 601–608.

Krissinel, E., and Henrick, K. (2007). Inference of macromolecular assemblies from crystalline state. J. Mol. Biol. *372*, 774–797.

Kyte, J., and Doolittle, R.F. (1982). A simple method for displaying the hydropathic character of a protein. J. Mol. Biol. *157*, 105–132.

Larkin, M.A., Blackshields, G., Brown, N.P., Chenna, R., McGettigan, P.A., McWilliam, H., Valentin, F., Wallace, I.M., Wilm, A., Lopez, R., et al. (2007). Clustal W and Clustal X version 2.0. Bioinformatics *23*, 2947–2948.

Leznicki, P., Clancy, A., Schwappach, B., and High, S. (2010). Bat3 promotes the membrane integration of tail-anchored proteins. J. Cell Sci. *123*, 2170–2178.

Liou, S.-T., and Wang, C. (2005). Small glutamine-rich tetratricopeptide repeat-containing protein is composed of three structural units with distinct functions. Arch. Biochem. Biophys. *435*, 253–263.

Liou, S.-T., Cheng, M.-Y., and Wang, C. (2007). SGT2 and MDY2 interact with molecular chaperone YDJ1 in *Saccharomyces cerevisiae*. Cell Stress Chaperones *12*, 59–70.

Mariappan, M., Li, X., Stefanovic, S., Sharma, A., Mateja, A., Keenan, R.J., and Hegde, R.S. (2010). A ribosome-associating factor chaperones tail-anchored membrane proteins. Nature *466*, 1120–1124.

Minami, R., Hayakawa, A., Kagawa, H., Yanagi, Y., Yokosawa, H., and Kawahara, H. (2010). BAG-6 is essential for selective elimination of defective proteasomal substrates. J. Cell Biol. *190*, 637–650.

Perrin, C.L., and Dwyer, T.J. (1990). Application of 2-dimensional NMR to kinetics of chemical exchange. Chem. Rev. *90*, 935–967.

Prag, G., Misra, S., Jones, E.A., Ghirlando, R., Davies, B.A., Horazdovsky, B.F., and Hurley, J.H. (2003). Mechanism of ubiquitin recognition by the CUE domain of Vps9p. Cell *113*, 609–620.

Saeki, Y., Saitoh, A., Toh-e, A., and Yokosawa, H. (2002). Ubiquitin-like proteins and Rpn10 play cooperative roles in ubiquitin-dependent proteolysis. Biochem. Biophys. Res. Commun. *293*, 986–992.

Sharma, D., and Rajarathnam, K. (2000). 13C NMR chemical shifts can predict disulfide bond formation. J. Biomol. NMR *18*, 165–171.

Sheinerman, F.B., Norel, R., and Honig, B. (2000). Electrostatic aspects of protein-protein interactions. Curr. Opin. Struct. Biol. *10*, 153–159.

Stevens, F.J. (1989). Analysis of protein-protein interaction by simulation of small-zone size exclusion chromatography. Stochastic formulation of kinetic rate contributions to observed high-performance liquid chromatography elution characteristics. Biophys. J. *55*, 1155–1167.

Tobaben, S., Varoqueaux, F., Brose, N., Stahl, B., and Meyer, G. (2003). A brain-specific isoform of small glutamine-rich tetratricopeptide repeat-containing protein binds to Hsc70 and the cysteine string protein. J. Biol. Chem. *278*, 38376–38383.

Wang, F., Brown, E.C., Mak, G., Zhuang, J., and Denic, V. (2010). A chaperone cascade sorts proteins for posttranslational membrane insertion into the endoplasmic reticulum. Mol. Cell *40*, 159–171.

Wang, Q., Liu, Y., Soetandyo, N., Baek, K., Hegde, R., and Ye, Y. (2011). A ubiquitin ligase-associated chaperone holdase maintains polypeptides in soluble states for proteasome degradation. Mol. Cell *42*, 758–770.

Winget, J.M., and Mayor, T. (2010). The diversity of ubiquitin recognition: hot spots and varied specificity. Mol. Cell *38*, 627–635.

Winnefeld, M., Grewenig, A., Schnölzer, M., Spring, H., Knoch, T.A., Gan, E.C., Rommelaere, J., and Cziepluch, C. (2006). Human SGT interacts with Bag-6/Bat-3/Scythe and cells with reduced levels of either protein display persistence of few misaligned chromosomes and mitotic arrest. Exp. Cell Res. *312*, 2500–2514.

Yang, F., Skaletsky, H., and Wang, P.J. (2007). Ubl4b, an X-derived retrogene, is specifically expressed in post-meiotic germ cells in mammals. Gene Expr. Patterns *7*, 131–136.